Article

Sub-ppb H_2S Sensing with Screen Printed Porous ZnO/SnO_2 Heterostructures

Mehdi Akbari-Saatlu *, Masoumeh Heidari, Claes Mattsson, Renyun Zhang, Göran Thungström

Posted Date: 8 October 2024

doi: 10.20944/preprints202410.0436.v1

Keywords: ZnO/SnO_2 heterostructure; gas sensor; H_2S; screen printing; ultrasonic spray pyrolysis

Article

Sub-ppb H_2S Sensing with Screen Printed Porous ZnO/SnO_2 Heterostructures

Mehdi Akbari-Saatlu *, Masoumeh Heidari, Claes Mattsson, Renyun Zhang and Göran Thungström

Department of Engineering, Mathematics and Science Education, Mid Sweden University, Holmgatan 10, SE-85170 Sundsvall, Sweden.

* Correspondence: author: mehdi.akbarisaatlu@miun.se

Abstract: Hydrogen sulfide (H_2S) is a highly toxic and corrosive gas commonly found in industrial emissions and natural gas processing, posing serious risks to human health and environmental safety even at low concentrations. Early detection of H_2S is therefore critical for preventing accidents and ensuring compliance with safety regulations. This study presents the development of porous ZnO/SnO_2 heterostructure gas sensors tailored for ultrasensitive detection of H_2S at sub-ppb levels. Utilizing a screen-printing method, we fabricated five different sensor compositions, ranging from pure SnO_2 to pure ZnO, and characterized their structural and morphological properties through X-ray diffraction (XRD) and scanning electron microscopy (SEM). Among these, sensor SnO_2/ZnO with composition weight ratio of 3:4 demonstrated highest response at 325 °C, achieving a low detection limit of 0.14 ppb. The sensor was evaluated for detecting H_2S concentrations ranging from 5 ppb to 500 ppb under dry, humid and N_2 conditions. The relative concentration error was carefully calculated based on analytical sensitivity, confirming the sensor's precision in measuring gas concentrations. Our findings underscore the significant advantages of heterostructure formation in enhancing gas sensitivity, offering promising applications in environmental monitoring and industrial safety. This research paves the way for the advancement of highly effective gas sensors capable of operating under diverse conditions with high accuracy.

KEYWORDS: ZnO/SnO_2 heterostructure; gas sensor; H_2S; screen printing; ultrasonic spray pyrolysis

1. Introduction

Metal oxide semiconductors have long been recognized as exceptional materials for gas sensing applications due to their high sensitivity to trace gas concentrations, stability, low cost, and potential for miniaturization and low power consumption [1]–[3]. However, while single metal oxide sensors offer broad gas detection capabilities, they often lack selectivity, presenting a significant challenge in distinguishing between different gases. To address this, recent research has focused on enhancing sensor selectivity through various methods, including doping with catalytic metals [4], surface modifications [5], and the development of multicompositional sensing films [6], [7].

One particularly promising approach involves the use of heterostructures composed of dissimilar metal oxides, such as ZnO and SnO_2 [8], [9]. These heterostructures leverage the formation of depletion layers at the junctions between different oxides, which can be modulated by the presence of target gases, thereby altering the sensor's conductivity [10]. Additionally, combining two different metal oxides can increase gas adsorption sites, further improving sensor performance [11], [12]. Among various combinations, ZnO/SnO_2 heterostructures have shown remarkable improvements in sensitivity and selectivity, particularly for detecting hazardous gases like hydrogen sulfide (H_2S) [13]–[15].

In previous studies, the authors have shown Ultrasonic Spray Pyrolysis (USP) can be used to deposit densely packed thin films of ZnO/SnO_2 heterostructures for H_2S detection [16]. These densely packed thin films achieved approximately 95 times better response than the pure SnO_2 sensor toward

 doi:10.20944/preprints202410.0436.v1

5 ppm H_2S at an operating temperature of 450 °C, with the lowest detection concentration of 0.5 ppm. Also in [17], Zhu et al. developed hierarchical and highly-ordered nanobowl ZnO/SnO_2 gas sensors, which demonstrated high sensitivity and selectivity for detecting H_2S gas at concentrations as low as 1 ppm, with long-term stability and repeatability. The hierarchical sensing materials were synthesized through a sequential process that involved hard template processing, atomic layer deposition, and hydrothermal processing. Additionally in [18], Guo et al. conducted a study on the hydrothermal synthesis of ZnO/SnO_2 for H_2S detection. Their findings showed that this type of heterostructure exhibits better H_2S gas response and selectivity compared to other interfering gases such as NO, SO_2, CO, CH_4, and C_2H_5OH. The most important works concerning gas sensing of ZnO/SnO_2 heterostructure have been summarized in [16].

H_2S is a highly toxic and flammable gas, characterized by its infamous rotten egg odor [19]. Even at low concentrations, H_2S poses significant health risks, including respiratory irritation, dizziness, and, at higher concentrations, can be fatal [20]. Additionally, H_2S is corrosive and can cause severe damage to equipment and infrastructure, particularly in industries such as petrochemicals, wastewater treatment, and natural gas processing [21]. The ability to accurately detect and monitor H_2S levels is therefore crucial for ensuring safety in both industrial and environmental settings. This drives the motivation to develop highly sensitive and selective sensors capable of detecting H_2S at very low concentrations.

In this study, ZnO/SnO_2 porous heterostructures were successfully fabricated using a screen-printing method with mayer-bar, producing five distinct sensor compositions ranging from pure SnO_2 to pure ZnO. The structural, morphological, and gas sensing properties of these sensors were thoroughly investigated. The heaters, essential for achieving the optimal operational temperature, were fabricated using USP, which enabled precise and uniform deposition on the sensor substrate. The study shows that the SnO_2/ZnO ratio 3:4 sensor composition demonstrated highest gas sensing performance among investigated samples towards low concentrations of H_2S (5 ppb). To quantitatively evaluate sensor performance, the concept of analytical sensitivity was employed. Analytical sensitivity provides a robust measure of the sensor's ability to detect small changes in gas concentration. This approach allows for the optimization of sensor signal selection and the direct calculation of potential errors in gas concentration measurements. The results of this study highlight the potential of screen printed porous ZnO/SnO_2 heterostructure thick films in developing highly efficient gas sensors with low detection limits and high sensitivity for various applications.

2. Experimental Details

The substrates used for fabricating SnO_2-ZnO porous heterostructure sensors were high-purity (99%) alumina plates, laser cut into small dimensions of 3 mm × 3 mm × 0.5 mm. Prior to any deposition, these substrates underwent a cleaning process involving ultrasonic baths in acetone and distilled water, followed by air drying.

For microheater formation, the cleaned alumina substrates were directly placed on the hot stage of an USP system, previously reported for various applications [22]–[24]. The precursor solution, consisting of 0.5 M stannous chloride dihydrate dissolved in 99.9% (v/v) ethanol, was prepared for USP deposition. The deposition process was carried out with a spray rate of 4 mL/min at a substrate temperature of 325°C for 30 minutes [25], [26]. Post-deposition, the samples were annealed at 900°C for one hour in air to stabilize the microheater characteristics, particularly for high-temperature operations.

The screen-printing method was employed to deposit the ZnO/SnO_2 sensing layers onto the substrates [27]. A homogeneous paste was prepared by grinding a mixture of SnO_2 and/or ZnO powder (Sigma-Aldrich, <100 nm particle size) with 1,2-propanediol (Sigma-Aldrich, 99.5+% ACS reagent) using a mortar. The resulting paste, with an oily/honey-like consistency, was coated onto the substrates using a mayer-bar coater equipped with a 16 μm grooved metallic bar. The bar was rolled over the alumina substrates at a speed of 20 mm/s, producing a uniform layer of the sensing material. The coated sensors were then left to settle at room temperature for 1 hour and subsequently

 doi:10.20944/preprints202410.0436.v1

dried on a hotplate at 80°C overnight. Finally, the sensors were annealed at 500°C for 10 minutes. The fabricated sensor details are listed in Table 1.

Table 1. Five distinct sensor compositions, ranging from pure SnO_2 to pure ZnO.

Sensors	Composition powder weight ratio	Explanation
S1	Pure SnO_2	Only SnO_2 powder
S2	ZnO/SnO_2 3:4	The weight of ZnO powder was three-quarters (3/4) of the weight of SnO_2 powder
S3	ZnO/SnO_2 1:1	The weight of SnO_2 powder was the same as the weight of ZnO powder
S4	SnO_2/ZnO 3:4	The weight of SnO_2 powder was three-quarters (3/4) of the weight of ZnO powder
S5	Pure ZnO	Only ZnO powder

The gas sensing properties of the fabricated sensors were evaluated in a controlled environment. The sensors were placed on a ceramic foundation equipped with electrical feedthroughs, housed within a stainless-steel chamber of 5 cm^3 volume. The chamber, maintained in a cleanroom environment, was fitted with connectors for gas inlet and outlet.

The gas flow was controlled using mass flow controllers (MFCs), with a continuous flow of 500±5 ml/min, monitored by an independent flowmeter. Precleaned and dried compressed air was used as the carrier gas. Target gas mixtures, including 100 ppm and 1 ppm H_2S diluted in N_2, were introduced from standard analytical quality gas cylinders. The relative humidity of the gas mixtures was continuously monitored using a commercial humidity sensor and adjusted with a bubble humidifier.

The sensors' operating temperature was held steady at 325 °C during measurements, with temperature monitored using small s-type thermocouple. A constant voltage of 5 V was applied, and electrical parameters were measured using Keithley 2410 electrometers. The entire experiment was controlled via LabVIEW software, with data acquisition at 0.5-second intervals.

3. Results and Discussion

The SEM images of the sensors (Figure 1a-Figure 1e) indicate porosity in all compositions, with a consistent film thickness of approximately 4-5 μm across the samples. The porous networks observed in the SEM micrographs are well-suited for gas diffusion. Additionally, the SEM image of the heaters (see Figure 1f) shows a uniform dense structure designed specifically by USP to provide efficient heating across the sensor surfaces.

The crystallographic phases of the fabricated ZnO/SnO_2 heterostructure sensors were analyzed by XRD, with distinct patterns observed for the pure ZnO and SnO_2 samples as well as their composites. According to Figure 1g, for the pure ZnO sample, the XRD pattern showed prominent diffraction peaks at 2θ values of 31.57°, 34.15°, 36.03°, 47.23°, and 56.35°, corresponding to the (100), (002), (101), (102), and (110) planes of the hexagonal wurtzite structure of ZnO (JCPDS No. 36-1451) [9], [28]. These peaks confirm the successful formation of highly crystalline ZnO with no other impurity phases present (the peaks are represented by red * in the XRD pattern of ZnO). The sharp and well-defined peaks indicate a high degree of crystallinity in the ZnO layer. In contrast, the pure SnO_2 sample exhibited diffraction peaks at 2θ values of 26.31°, 33.65°, 51.5°, and 54.57° corresponding to the (110), (101), (211), and (220) planes, respectively. These reflections are characteristic of the tetragonal rutile phase of SnO_2 (JCPDS No. 41-1445), confirming the high crystallinity of the SnO_2 component (the peaks are represented by green° in the XRD pattern of SnO_2) [29], [30].

 doi:10.20944/preprints202410.0436.v1

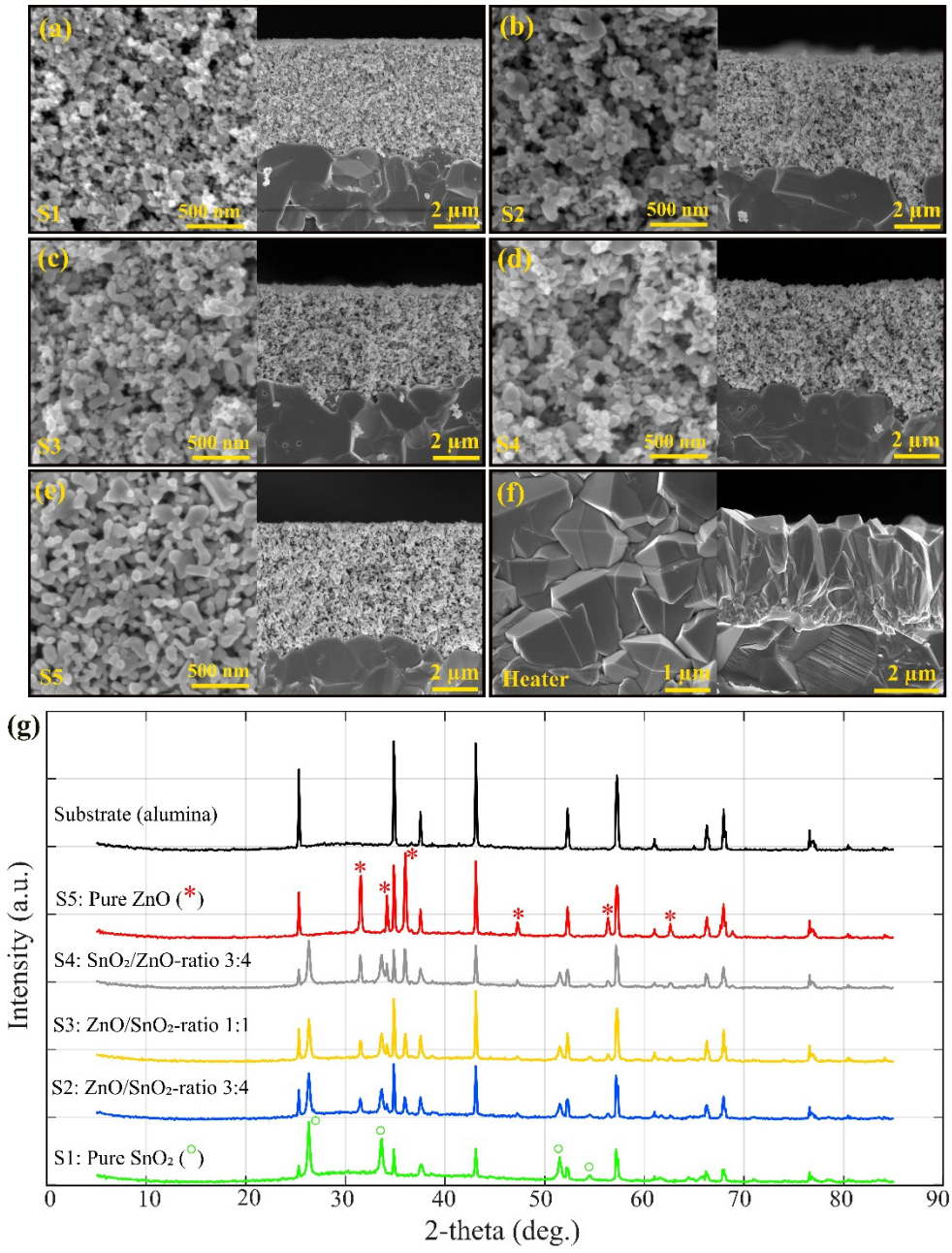

Figure 1. Plan view and the cross-sectional SEM micrographs of the porous thick film sensors prepared by mayer-bar coater on alumina substrate: (a) S1 pure SnO_2, (b) S2, (c) S3, (d) S4, (e) S5 pure ZnO, and (f) SnO_2 densely packed thick films microheaters prepared by USP and (g) θ–2θ diffractograms from sensors S1 to S5 as well as alumina substrate.

In the composite sensors, the XRD patterns reflected a combination of the distinct ZnO and SnO_2 peaks, depending on the ZnO and SnO_2 ratio. For instance, in the S4 (SnO_2/ZnO, ratio 3:4) sample, peaks from both the hexagonal ZnO and the tetragonal SnO_2 phases were detected, indicating the coexistence of both materials without significant phase interaction or formation of secondary compounds. The preservation of these individual crystalline phases suggests that the heterostructures were formed via a simple physical mixing of the ZnO and SnO_2 phases without solid-state reaction at the temperatures used in this study. The heterostructure sample S4, which exhibited both the ZnO and SnO_2 diffraction peaks, showed the highest H_2S gas response, suggesting that the presence of both phases is essential for enhancing gas sensing performance through the creation of additional active sites and improved charge transfer at the interface in the presence of target gas.

 doi:10.20944/preprints202410.0436.v1

In order to determine the optimal operating temperature, sensor S3 was exposed to 5 ppm of H_2S for 5 minutes at varying temperatures, ranging from 200 °C to 450 °C (at 5% RH). The highest sensor response was observed at 325 °C, which this temperature is lower than our previous findings on ZnO/SnO_2 heterostructures prepared by USP [16]. As illustrated in Figure 2a, all sensors were subsequently tested at this optimal operating temperature towards 5 ppm of H_2S for 5 minutes under dry conditions (5% RH). The results indicate that sensor S4 exhibited the highest response among the investigated samples and was therefore selected for further investigation. Interestingly, in all compositions containing both ZnO and SnO_2 (S2, S3, S4), the response was higher than that of the pure SnO_2 (S1) and pure ZnO (S5) samples, highlighting the critical role of heterostructures in enhancing the sensor's response to the target gas.

The dynamic response (R_g) of the sensor (S4) to H_2S gas is illustrated in Figure 2b. The sensor is exposed to varying concentrations of H_2S (5 ppb, 10 ppb, 50 ppb, 200 ppb, and 500 ppb) at 325 °C for 30 minutes in 5% RH, followed by a 2-hour recovery period. The sensor (S4) exhibited approximately 10, 12, 28, 60, and 82 times changes in resistance (R_o/R_g) upon exposure to 5 ppb, 10 ppb, 50 ppb, 200 ppb, and 500 ppb of H_2S, respectively. These values (detection levels, concentrations) are significantly lower than those reported in previous studies [13], [16].

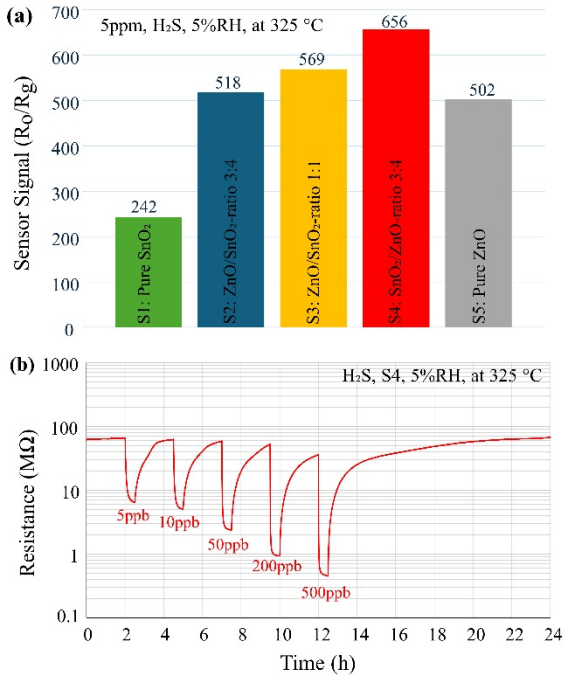

Figure 2. (a) Sensor signal (R_o/R_g) of all sensors (S1 to S5) towards 5 ppm of H_2S. (b) Dynamic response (R_g) of the sensor S4 to different concentrations of H_2S (5, 10, 50, 200, 500 ppb, exposure time is 30 min) in dry condition (5%RH).

In gas sensing, the sensor response can be defined either by the relative change in resistance (R_o/R_g) or directly by the resistance in the presence of the target gas (R_g). The choice of signal significantly affects the accuracy and reliability of the sensor readings.

The 6 measured points and corresponding fitting curves (sensor signal vs concentration) for R_g and R_o/R_g are presented in Figure 3a and 3b. To further investigate the sensor signal, analytical sensitivity (sensitivity over standard division of sensor signal) is calculated and presented in Figure 3c, indicating higher values for R_g compared to R_o/R_g in all concentration. In this Figure both curves related to analytical sensitivity decreasing gradually by increasing concentration.

Analysis of the sensor's performance reveals that using R_o/R_g leads to higher error bars compared to R_g. This is primarily due to variations in the baseline resistance (R_o), which can introduce significant inaccuracies, particularly at low concentrations. To be more precise, the relative concentration error can be calculated using analytical sensitivity. As demonstrated in Figure 3d, the relative concentration error with R_o/R_g reached up to 14% at 5 ppb, highlighting substantial

 doi:10.20944/preprints202410.0436.v1

measurement uncertainties. Conversely, when R_g is used as the sensor signal, the influence of baseline fluctuations is minimized, resulting in a more stable and accurate detection of the target gas. This approach yields lower relative concentration errors, generally less than 6% across all tested concentrations (5 ppb to 500 ppb), and reaching around 1% relative concentration error at 500ppb, as illustrated in Figure 3d. The improved precision with R_g underscores its advantage over R_o/R_g in reducing measurement errors and enhancing sensor performance. Thus, selecting R_g as the sensor signal is crucial for achieving a more accurate and reliable response. By mitigating baseline-related inaccuracies, R_g provides a more effective measurement of target gases, ensuring higher sensitivity and precision in gas detection applications.

To examine the effect of humidity, the same measurements were performed at 50% RH, and the results, along with the fitted curves, are shown in Figure 3a and 3b. The data indicates that higher humidity levels cause changes in the sensor's resistance. However, when using the sensor's resistance (R_g) as the sensor signal, the slope of the calibration curve, or sensitivity, in humid conditions remains almost the same as in dry conditions. On the other hand, when using R_o/R_g as the sensor signal, the sensitivity changes significantly under humid conditions compared to the dry state (5% RH). In humid environments, H_2S molecules must compete with water molecules for adsorption sites on the pre-adsorbed oxygen species. This suggests that in humid conditions, fewer sites are available for H_2S molecules to adsorb and contribute to the sensor's conductivity.

Following the approach detailed in [31], the LOD for S4 (5%RH, at 325 °C) was calculated by extrapolating the fitted calibration curve to its intersection with a signal level equivalent to three times the standard deviation of the noise level. Specifically, the LOD for H_2S was determined to be 0.14 ppb. These calculations demonstrate the sensitivity of the sensor and its capability to detect low concentrations of these gases with a high degree of confidence.

Preprints.org (www.preprints.org) | NOT PEER-REVIEWED | Posted: 8 October 2024 doi:10.20944/preprints202410.0436.v1

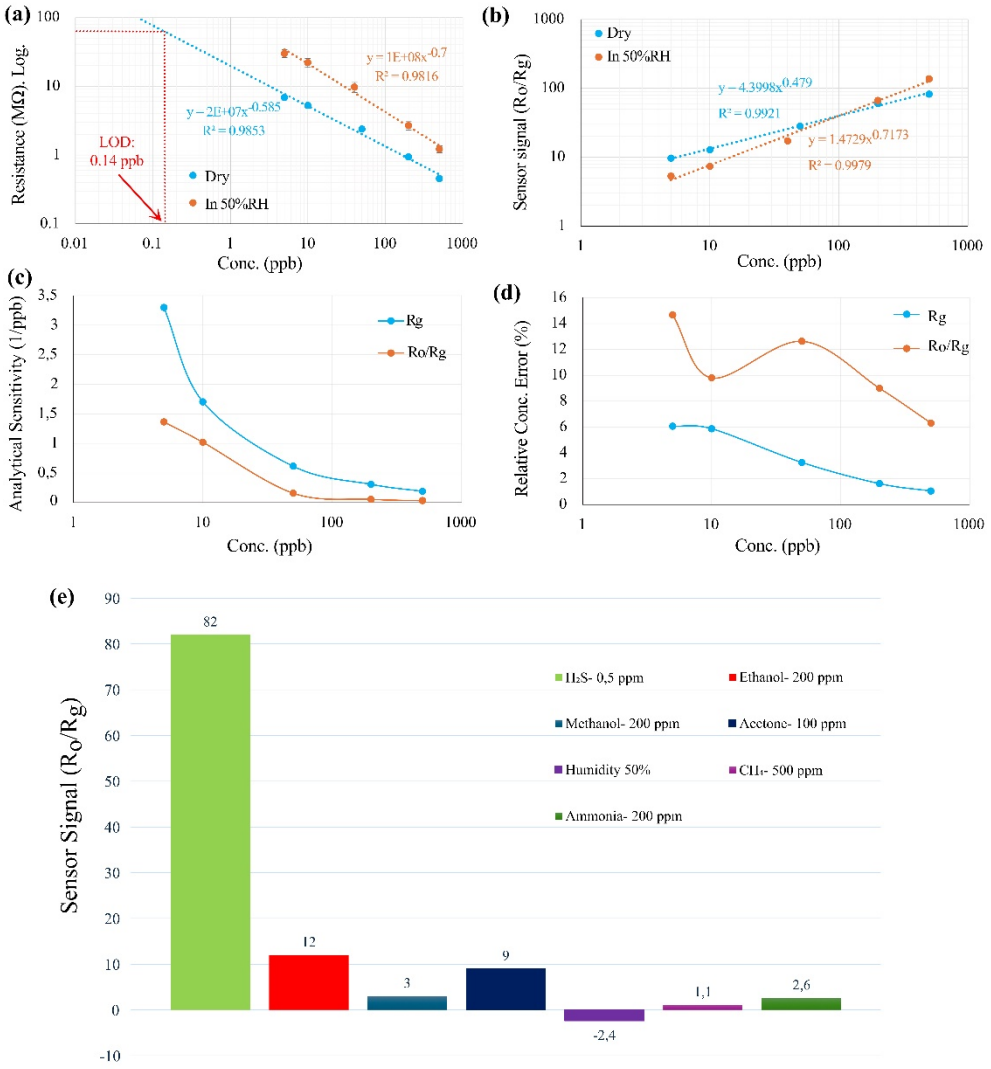

Figure 3. The fitting curve of the sensor S4 in response to H_2S (5 ppb to 500 ppb) under dry (5%RH) and humid condition (50%RH) for the (a) resistance of the sensor (R_g) and (b) relative changes of the resistance (R_o/R_g). (c) Calculated analytical sensitivity in dry condition and (d) corresponding relative concentration error. (e) Selectivity of the S4 towards some interfering gases at 325 °C (5 %RH).

Sensing Mechanism

Oxygen plays an essential role in redox reactions on the surface of metal oxides [32]. When the sensor is exposed to air, oxygen molecules are absorbed on its surface, leading to the formation of reactive oxygen species such as O_2^-, O^-, and O^{2-} [33], [34]. These species are formed as electrons move from the metal oxide surface to the adsorbed oxygen, causing the surface to oxidize and resulting in upward band bending in the energy diagram. At 325 °C, O^- is the main species on the surface. When the sensor comes into contact with a reducing gas like H_2S, these oxygen species react with the gas, releasing electrons into the sensing material. The reaction can be written as:

$$H_2S + 3O^-_{(ads)} \rightarrow SO_2 + H_2O + 3e^- \quad \text{at } 325\ ^\circ C$$

This reaction increases the number of free electrons on the surface, thereby reducing the sensor's resistance. In the presence of air, a depletion layer forms on the ZnO/SnO_2 grains, primarily controlled by negatively charged oxygen species. Electrons must overcome the barrier between the heterostructure and homostructure grains (ZnO grains, SnO_2 grains, and ZnO/SnO_2 grains, see Figure 4a and also related energy band diagram are presented in Figure 4b) to contribute to electrical conduction. The baseline resistance of the heterostructure (ZnO/SnO_2) is significantly higher than that of the pure ZnO or SnO_2, indicating the existence of an energy barrier between the dissimilar

 doi:10.20944/preprints202410.0436.v1

metal oxide grains. This barrier results from the difference in work functions and electron affinity between ZnO and SnO_2, which creates a built-in potential, leading to a depletion region at the interface [11].

When the sensor is exposed to H_2S, the adsorbed oxygen species on the surface of ZnO/SnO_2 grains react with the gas molecules, releasing free electrons. In addition, thanks to the porous structures prepared by screen printing H_2S can penetrate into the sensing layer and interact with hole sensing layer. This interaction reduces the thickness of the depletion layer (see Figure 4a) and lowers the barrier at the heterostructure interface, allowing electrons to flow more easily across the grain boundaries. As the barrier decreases, the resistance of the sensor drops, leading to an increase in current flow. This is especially evident in ZnO/SnO_2 heterostructures, where the combination of both materials enhances the sensitivity and response to H_2S by providing additional active sites for gas interaction.

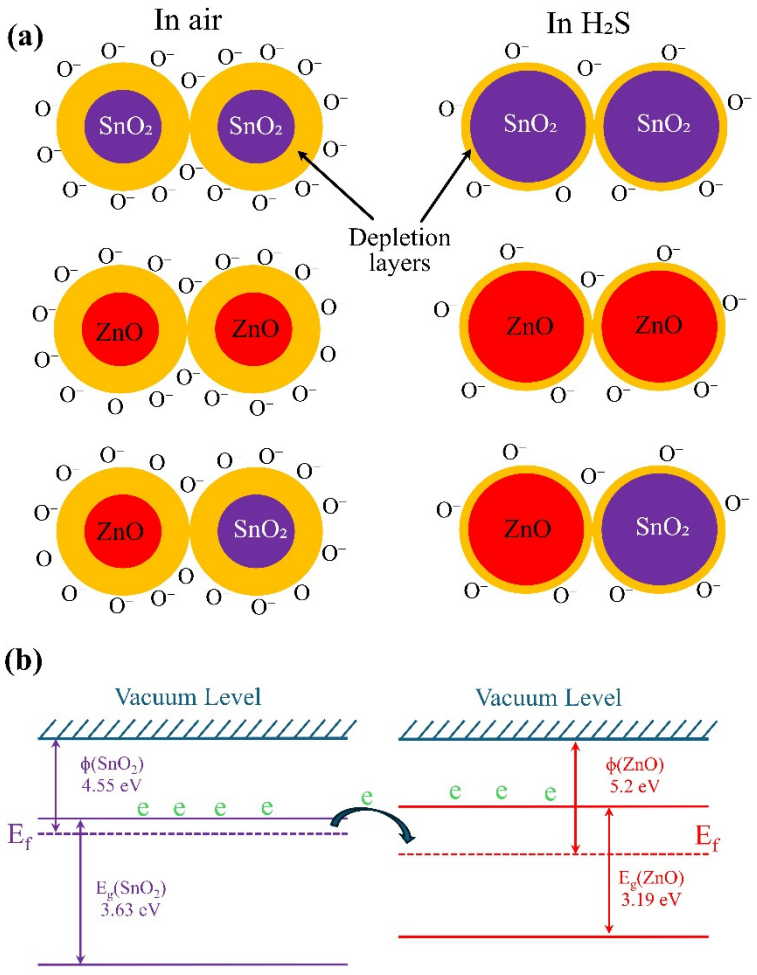

Figure 4. (a) Gas sensing mechanism in air and H_2S, (b) energy band diagram of ZnO and SnO_2 at equilibrium state before contact and after contact fermi levels will be equal.

For ZnO/SnO_2 porous structures made using screen printing, in the presence of N_2, the number of free charge carriers involved in conduction is equal to the number of free charge carriers in the bulk material. As a result, by this consideration there is no initial band bending, and the sensor's resistance in N_2 sets the threshold between conduction mechanisms controlled by the depletion layer and the accumulation layer [35], [36]. For the S4 sensor, this boundary is measured at 766 kΩ (the sensor's resistance in N_2, see Figure S1 in supplementary information).

In dry air, as the concentration of the target gas increases, the sensor's resistance decreases. For H_2S concentrations higher than 260 ppb (according to the calibration curve), the conduction

 doi:10.20944/preprints202410.0436.v1

mechanism shifts from being controlled by the depletion layer to the accumulation layer. However, in humid conditions (50% RH), across all investigated H_2S concentrations (5 ppb to 500 ppb), the conduction remains controlled by the depletion layer, with no transition to the accumulation layer observed. However, according to the calibration curve (in 50% RH) for concentrations higher than 1 ppm the conduction mechanism will shift to the region controlled by accumulation layer.

The sensor's selectivity towards some common interfering gases like ethanol, CH_4, methanol, acetone, ammonia, and humidity were investigated, and the results are presented in Figure 3e.

4. Conclusions

This research successfully developed ZnO/SnO_2 porous heterostructure gas sensors for the detection of H_2S, with sensor S4 (SnO_2/ZnO ratio 3:4) showing the best performance among the tested compositions. The sensor demonstrated high sensitivity at 325°C and a low detection limit (LOD) of 0.14 ppb, with the ability to detect H_2S concentrations as low as 5 ppb. The relative concentration error, calculated based on analytical sensitivity, confirmed the precision of the sensor's response by choosing the right sensor signal. Compared to pure SnO_2 and ZnO sensors, the heterostructure-based sensors exhibited enhanced gas sensing performance. The sensor's stable performance under both dry and humid conditions makes it promising for real-world applications. These findings provide a solid basis for the development of advanced gas sensors with high accuracy and low detection limits.

Supplementary Materials: The following supporting information can be downloaded at the website of this paper posted on Preprints.org.

References

1. D. Meng *et al.*, "In Situ Fabrication of SnS2/SnO2 Heterostructures for Boosting Formaldehyde–Sensing Properties at Room Temperature," *Nanomater. 2023, Vol. 13, Page 2493*, vol. 13, no. 17, p. 2493, Sep. 2023, doi: 10.3390/NANO13172493.
2. B. Y. Song *et al.*, "Highly selective ppb-level H2S sensor for spendable detection of exhaled biomarker and pork freshness at low temperature: Mesoporous SnO2 hierarchical architectures derived from waste scallion root," *Sensors Actuators, B Chem.*, vol. 307, p. 127662, Mar. 2020, doi: 10.1016/j.snb.2020.127662.
3. M. Akbari-Saatlu *et al.*, "Ultra-sensitive H2S and CH3SH Sensors Based on SnO2 Porous Structures Utilizing Combination of Flame and Ultrasonic Spray Pyrolysis Methods," *IEEE Sens. J.*, 2024, doi: 10.1109/JSEN.2024.3467168.
4. L. Zhao *et al.*, "Increasing the Catalytic Activity of Co3O4 via Boron Doping and Chemical Reduction for Enhanced Acetone Detection," *Adv. Funct. Mater.*, vol. 34, no. 18, p. 2314174, May 2024, doi: 10.1002/ADFM.202314174.
5. C. Wang *et al.*, "Pt-modified nanosheet-assembled SnS2 hollow microspheres for low temperature NO2 sensors," *Sensors Actuators B Chem.*, vol. 417, p. 136118, Oct. 2024, doi: 10.1016/J.SNB.2024.136118.
6. H. Xia, D. Zhang, Y. Sun, J. Wang, and M. Tang, "Ultrasensitive H2S Gas Sensor Based on SnO2 Nanoparticles Modified WO3 Nanocubes Heterojunction," *IEEE Sens. J.*, vol. 23, no. 22, pp. 27031–27037, Nov. 2023, doi: 10.1109/JSEN.2023.3321726.
7. J. Hu *et al.*, "An olive-shaped SnO2 nanocrystal-based low concentration H2S gas sensor with high sensitivity and selectivity," *Phys. Chem. Chem. Phys.*, vol. 17, no. 32, pp. 20537–20542, Aug. 2015, doi: 10.1039/C5CP02854J.
8. T. Li *et al.*, "The Combination of Two-Dimensional Nanomaterials with Metal Oxide Nanoparticles for Gas Sensors: A Review," *Nanomater. 2022, Vol. 12, Page 982*, vol. 12, no. 6, p. 982, Mar. 2022, doi: 10.3390/NANO12060982.
9. S. D. Patil *et al.*, "Highly selective ppm level LPG sensors based on SnO2-ZnO nanocomposites operable at

low temperature," *Sensors Actuators B Chem.*, vol. 377, p. 133080, Feb. 2023, doi: 10.1016/J.SNB.2022.133080.

10. X. Ren, Z. Xu, Z. Zhang, and Z. Tang, "Enhanced NO2 Sensing Performance of ZnO-SnO2 Heterojunction Derived from Metal-Organic Frameworks," *Nanomaterials*, vol. 12, no. 21, p. 3726, Nov. 2022, doi: 10.3390/NANO12213726/S1.
11. M. H. Raza *et al.*, "Role of Heterojunctions of Core–Shell Heterostructures in Gas Sensing," *ACS Appl. Mater. Interfaces*, vol. 14, no. 19, pp. 22041–22052, May 2022, doi: 10.1021/ACSAMI.2C00808/ASSET/IMAGES/LARGE/AM2C00808_0005.JPEG.
12. Z. Wang, P. Li, B. Feng, Y. Feng, D. Cheng, and J. Wei, "Wireless Gas Sensor Based on the Mesoporous ZnO-SnO2 Heterostructure Enables Ultrasensitive and Rapid Detection of 3-Methylbutyraldehyde," *ACS Sensors*, vol. 9, no. 5, pp. 2585–2595, May 2024, doi: 10.1021/ACSSENSORS.4C00306/ASSET/IMAGES/LARGE/SE4C00306_0006.JPEG.
13. D. Fu, C. Zhu, X. Zhang, C. Li, and Y. Chen, "Two-dimensional net-like SnO2/ZnO heteronanostructures for high-performance H2S gas sensor," *J. Mater. Chem. A*, vol. 4, no. 4, pp. 1390–1398, Jan. 2016, doi: 10.1039/C5TA09190J.
14. B. W. Hwang *et al.*, "High sensitivity and recoverable SnO2-based sensor promoted with Fe2O3 and ZnO for sub-ppm H2S detection," *J. Nanoelectron. Optoelectron.*, vol. 12, no. 6, pp. 617–621, Jun. 2017, doi: 10.1166/JNO.2017.2062.
15. S. C. Lee *et al.*, "New SnO2-based gas sensor promoted with ZnO and MoO3 for the detection of H2S," *Sens. Lett.*, vol. 12, no. 6–7, pp. 1181–1185, Jun. 2014, doi: 10.1166/SL.2014.3190.
16. M. Akbari-Saatlu *et al.*, "Nanometer-Thick ZnO/SnO2Heterostructures Grown on Alumina for H2S Sensing," *ACS Appl. Nano Mater.*, vol. 5, no. 5, pp. 6954–6963, May 2022, doi: 10.1021/ACSANM.2C00940/ASSET/IMAGES/LARGE/AN2C00940_0007.JPEG.
17. L.-Y. Zhu *et al.*, "Hierarchical highly ordered SnO2 nanobowl branched ZnO nanowires for ultrasensitive and selective hydrogen sulfide gas sensing," *Microsystems Nanoeng. 2020 61*, vol. 6, no. 1, pp. 1–13, May 2020, doi: 10.1038/s41378-020-0142-6.
18. W. Guo, L. Mei, J. Wen, and J. Ma, "High-response H2S sensor based on ZnO/SnO2 heterogeneous nanospheres," *RSC Adv.*, vol. 6, no. 18, pp. 15048–15053, Feb. 2016, doi: 10.1039/C5RA22187K.
19. M. Akbari-Saatlu *et al.*, "Silicon Nanowires for Gas Sensing: A Review," *Nanomaterials*, vol. 10, no. 11, p. 2215, Nov. 2020, doi: 10.3390/nano10112215.
20. M. Hussain, M. O'Nils, J. Lundgren, M. A. Saatlu, R. Hamrin, and C. Mattsson, "A Deep Learning Approach for Classification and Measurement of Hazardous Gases Using Multi-Sensor Data Fusion," *2023 IEEE Sensors Appl. Symp. SAS 2023 - Proc.*, 2023, doi: 10.1109/SAS58821.2023.10254191.
21. F. Hossein-Babaei, S. Masoumi, S. Aghili, and M. Shokrani, "Atmospheric Dependence of Thermoelectric Generation in SnO2Thin Films with Different Intergranular Potential Barriers Utilized for Self-Powered H2S Sensor Fabrication," *ACS Appl. Electron. Mater.*, vol. 3, no. 1, pp. 353–361, Jan. 2021, doi: 10.1021/acsaelm.0c00893.
22. F. Hossein-Babaei and M. Akbari-Saatlu, "Growing continuous zinc oxide layers with reproducible nanostructures on the seeded alumina substrates using spray pyrolysis," *Ceram. Int.*, vol. 46, no. 7, pp. 8567–8574, May 2020, doi: 10.1016/j.ceramint.2019.12.088.
23. F. Hossein-Babaei and M. Akbari-Saatlu, "Growth of ZnO nanorods on the surface and edges of a multilayer graphene sheet," *Scr. Mater.*, vol. 139, pp. 77–82, Oct. 2017, doi: 10.1016/j.scriptamat.2017.06.025.
24. S. Masoumi, M. Shokrani, S. Aghili, and F. Hossein-Babaei, "Zinc oxide-based direct thermoelectric gas sensor for the detection of volatile organic compounds in air," *Sensors Actuators, B Chem.*, vol. 294, pp. 245–

252, Sep. 2019, doi: 10.1016/j.snb.2019.05.063.

25. F. Hossein-Babaei, M. Gharesi, and M. Ansari, "Ten micron-thick undoped SnO2 layers grown by spray pyrolysis for microheater fabrication," *Mater. Lett.*, vol. 196, pp. 104–107, Jun. 2017, doi: 10.1016/J.MATLET.2017.03.015.
26. F. Hossein-Babaei and M. Gharesi, "Intense thermal shock generators made of micron-thick SnO2 layers for the on-chip rapid thermal processing in air," *Mater. Today Commun.*, vol. 39, p. 108719, Jun. 2024, doi: 10.1016/J.MTCOMM.2024.108719.
27. C. E. Simion, B. Junker, U. Weimar, A. Stanoiu, and N. Bârsan, "Sensing mechanisms of CO and H2 with NiO material – DRIFTS investigations," *Sensors Actuators B Chem.*, vol. 390, p. 134028, Sep. 2023, doi: 10.1016/J.SNB.2023.134028.
28. D. Raoufi and T. Raoufi, "The effect of heat treatment on the physical properties of sol–gel derived ZnO thin films," *Appl. Surf. Sci.*, vol. 255, no. 11, pp. 5812–5817, Mar. 2009, doi: 10.1016/J.APSUSC.2009.01.010.
29. S. B. Dhage, V. L. Patil, A. M. Yelpale, and Y. S. Malghe, "Farming of ZnO–SnO2 Nanocubes for Chemiresistive NO2 Gas Detection," *ChemistrySelect*, vol. 9, no. 1, p. e202303578, Jan. 2024, doi: 10.1002/SLCT.202303578.
30. K. Hu, J. Zhang, Y. He, R. Yan, and J. Li, "Hydrogenation effect on 2D ZnO single crystal/ZnO–SnO2 two phase ceramics and its enhanced mechanism in H2 gas sensing," *Ceram. Int.*, vol. 50, no. 4, pp. 6441–6452, Feb. 2024, doi: 10.1016/J.CERAMINT.2023.11.384.
31. A. D'amico and C. Di Natale, "A Contribution on Some Basic Definitions of Sensors Properties," *IEEE Sens. J.*, vol. 1, no. 3, p. 183, 2001.
32. D. Degler, U. Weimar, and N. Barsan, "Current Understanding of the Fundamental Mechanisms of Doped and Loaded Semiconducting Metal-Oxide-Based Gas Sensing Materials," *ACS Sensors*, vol. 4, no. 9, pp. 2228–2249, Sep. 2019, doi: 10.1021/ACSSENSORS.9B00975/ASSET/IMAGES/LARGE/SE9B00975_0022.JPEG.
33. R. T. Ghahrizjani *et al.*, "Highly sensitive H2S gas sensor containing simultaneously UV treated and self-heated Ag-SnO2 nanoparticles," *Sensors Actuators B Chem.*, vol. 391, p. 134045, Sep. 2023, doi: 10.1016/J.SNB.2023.134045.
34. L. Mei, Y. Chen, and J. Ma, "Gas Sensing of SnO2 Nanocrystals Revisited: Developing Ultra-Sensitive Sensors for Detecting the H2S Leakage of Biogas," *Sci. Reports 2014 41*, vol. 4, no. 1, pp. 1–8, Aug. 2014, doi: 10.1038/srep06028.
35. N. Bârsan, M. Hübner, and U. Weimar, "Conduction mechanisms in SnO2 based polycrystalline thick film gas sensors exposed to CO and H2 in different oxygen backgrounds," *Sensors Actuators B Chem.*, vol. 157, no. 2, pp. 510–517, Oct. 2011, doi: 10.1016/J.SNB.2011.05.011.
36. A. Staerz, U. Weimar, and N. Barsan, "Current state of knowledge on the metal oxide based gas sensing mechanism," *Sensors Actuators B Chem.*, vol. 358, p. 131531, May 2022, doi: 10.1016/J.SNB.2022.131531.